The relationships between volcanism and extension in the Mesa Central: the case of Pinos, Zacatecas, Mexico

José Jorge Aranda-Gómez[1,*], Roberto Molina-Garza[1], Fred W. McDowell[2], Luis Fernando Vassallo-Morales[1], María Amabel Ortega-Rivera[3], José Gregorio Solorio-Munguía[1], and Alfredo Aguillón-Robles[4]

[1] *Centro de Geociencias, Universidad Nacional Autónoma de México, Campus Juriquilla, 76230 Querétaro, Qro., Mexico.*
[2] *Department of Geological Sciences, The University of Texas at Austin, 1 University Station C1100, Austin, TX 78712, USA.*
[3] *Instituto de Geología, Universidad Nacional Autónoma de México, Apartado Postal 1039, 83000 Hermosillo, Son., Mexico.*
[4] *Instituto de Geología, Universidad Autónoma de San Luis Potosí, Av. Manuel Nava 5, Zona Universitaria, 78240 San Luis Potosí, S.L.P., Mexico.*
* jjag@geociencias.unam.mx

ABSTRACT

Pinos volcanic complex is an uplifted area that exposes Mesozoic strata and mid-Tertiary volcanic and sedimentary rocks. Its stratigraphy, deformation style, and volcanism are characteristic of the Mesa Central region of central Mexico and the southeastern segment of the Sierra Madre Occidental (SMO) volcanic province. The oldest rocks in Pinos are marine carbonate sedimentary and siliciclastic rocks that underlie a red bed sequence (Pinos red beds) interlayered with felsic volcanic rocks, in turn partially covered by a voluminous lava dome complex. The Pinos red bed sequence is at least 900 m thick and it is formed by well-lithified conglomeratic sandstone and matrix-supported, generally fine-grained to medium-grained, polymictic conglomerate. Clasts in the Pinos red beds were derived from the Mesozoic basement, subaerial felsic volcanic rocks of unknown provenance, and tourmaline-bearing muscovite granite. Interlayered volcanic rocks include ash-fall tuffs, a densely welded ash-flow tuff, and water-laid or reworked pyroclastic material. The main components of the dome complex are a dark-red, porphyritic potassium-rich trachyte, and a buff-colored, porphyritic rhyolite, for which we report lava mingling (the first one in the SMO volcanic province). Field relations at the Pinos volcanic complex demonstrate a close temporal relationship between felsic volcanism and extension. Faulting in Pinos is complex as it includes arrays of Cenozoic normal faults with NS, NW, and NE trends, for which cross-cutting relations are ambiguous. A combination of mapping, K-Ar geochronology, petrographic work and interpretation of the magnetic polarity of the volcanic units allow us to establish that repeated pulses of synextensional volcanism occurred during the period between ~32 and 27 Ma. These data demonstrate that extension in the Mesa Central is older than 29–27 Ma, the oldest previously recognized episode of extension. The earliest (≥ 32 Ma) pulse of extension may be related to a regional (~250 km long) NW-trending fault system that divides the Mesa Central into two domains with contrasting stratigraphy and different geomorphic aspect. The Pinos red bed sequence includes clasts of the Peñón Blanco granite ($^{40}Ar/^{39}Ar$ = 50.94 ± 0.47 Ma), that in addition to providing a minimum age for the end of the Laramide orogeny in the Mesa Central, offers evidence of uplift and denudation of the granite before or synchronous with red bed deposition.

Key words: extension, volcanism, magma mingling, volcanic domes, red beds, Basin and Range, Sierra Madre Occidental, Pinos, Mexico.
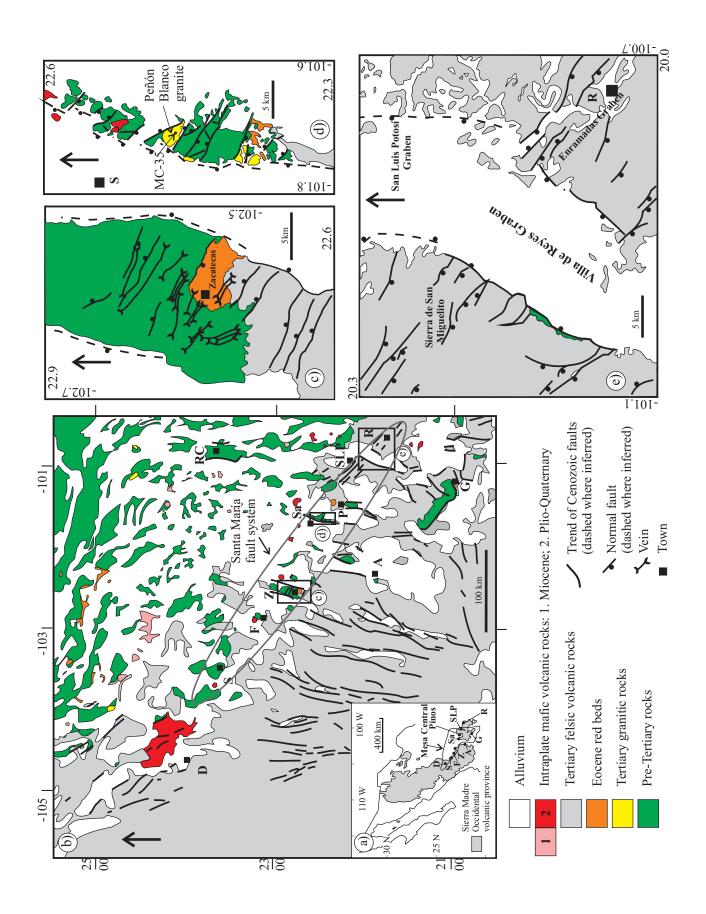
RESUMEN

El complejo volcánico de Pinos es una región elevada en donde están expuestas rocas sedimentarias mesozoicas y rocas volcánicas y sedimentarias del Terciario medio. Su estratigrafía, estilo de deformación y volcanismo son característicos de la Mesa Central de México, así como de la porción sureste de la provincia volcánica de la Sierra Madre Occidental (SMO). Las rocas más antiguas expuestas en Pinos son rocas sedimentarias carbonatadas y siliciclásticas que subyacen a una secuencia de capas rojas intercaladas con rocas volcánicas félsicas, que a su vez son cubiertas por un complejo de domos volcánicos voluminosos. Las capas rojas de Pinos tienen un espesor mínimo de 900 m y están compuestas por areniscas conglomeráticas bien litificadas y por capas de conglomerado polimíctico soportado por matriz, con tamaños de grano que varían de medio a fino. Los clastos de las capas rojas de Pinos provienen del basamento Mesozoico, de rocas volcánicas continentales de composición félsica y proveniencia desconocida, y de un granito con moscovita y turmalina. Tobas félsicas de caída, una ignimbrita densamente soldada y material piroclástico retrabajado se encuentran intercalados con las capas rojas. Los componentes principales del complejo de domos –en los que reconocimos mezcla inhomogénea (mingling) de magmas (el primer caso documentado en la provincia volcánica de la SMO)– son derrames de traquita de color rojo oscuro y de riolita porfídica de color paja. Las relaciones de campo en el complejo de Pinos demuestran una asociación temporal muy cercana entre el volcanismo félsico y el fallamiento normal en la región. El fallamiento en Pinos es complejo, ya que incluye conjuntos de fallas con orientaciones NS, NW y NE con relaciones de corte que en conjunto rinden una cronología ambigua. Una combinación de cartografía geológica, geocronología K-Ar, petrografía y análisis de la polaridad magnética de las unidades volcánicas nos permitió establecer que hubo varios pulsos de deformación contemporáneos al volcanismo en el período comprendido entre ~32 y 27 Ma. Esta información muestra que el fallamiento normal en la Mesa Central es más antiguo que 29–27 Ma, la edad del pulso de deformación más antiguo previamente identificado. El primer pulso de deformación en la región (≥32 Ma) posiblemente está relacionado con un sistema de fallas regional (≥250 km de longitud) con orientación NW y que divide a la Mesa Central en dos dominios con estratigrafía y aspecto geomorfológico distinto. Las capas rojas de Pinos incluyen clastos del granito del Peñón Blanco ($^{40}Ar/^{39}Ar$ = 50.94 ± 0.47 Ma), que además de proporcionar una edad mínima para la deformación laramídica en el área, son evidencia de la edad del levantamiento y denudación del granito, previo o contemporáneo con la acumulación de las capas rojas.

Palabras clave: extensión, volcanismo, mezcla inhomogénea de magmas, domos volcánicos, capas rojas, Cuencas y Sierras, Sierra Madre Occidental, Pinos, México.

INTRODUCTION

In this paper we try to unravel the timing of formation of the mid-Tertiary Pinos volcanic complex in Central Mexico (Figure 1a) and its relation to synvolcanic faulting and sedimentation. The chosen topic is important because the Pinos volcanic complex is part of the Sierra Madre Occidental (SMO) volcanic field (Figure 1a), the world´s largest accumulation of felsic ignimbrites and lava flows (McDowell and Keizer, 1977). Recent papers have pointed out the importance of the close relation between normal faulting and volcanic activity in the SMO (*e.g.*, Aguirre-Díaz and McDowell, 1993; Aranda-Gómez *et al.*, 1997, 2000; Nieto-Samaniego *et al.*, 1999; Orozco-Esquivel, *et al.*, 2002; Ferrari *et al.*, 2002). However, for the most part, the inferred synextensional character of the volcanism is based on comparatively few detailed field studies and in a compilation of rather sparse K-Ar ages (*e.g.*, Nieto-Samaniego *et al.*, 1999). It is fairly well established that extensional tectonics in the Mesa Central, located at the SE portion of the SMO (Figure 1a), occurred in several pulses: ~29–27 Ma, ~24 Ma,

and ~11 Ma (Nieto-Samaniego *et al.*, 1999), also observed in other regions of the SMO (Aranda-Gómez *et al.*, 1997, 2000). An earlier period of extension (mid-Eocene to early Oligocene) has been inferred in the Mesa Central from the study of continental red bed sequences underlying the mid-Tertiary volcanic rocks (Edwards, 1955; Aranda-Gómez and McDowell, 1998).

The Pinos volcanic complex is also important because it is located immediately south of the regional NW-trending Río Santa María normal fault system (Figure 1b), which extends for more than 250 km across or at the southwestern boundary the Mesa Central (*e.g.*, Nieto-Samaniego *et al.*, 2005). This fault system, in places more than 20 km wide, was first identified by Labarthe-Hernández *et al.* (1987, 1989) in the hydrological basin of the Río Santa María (Figures 1a, 1b, 1e) near El Realito fluorite mine. It includes a well-defined domino-type array of faults in the Sierra de San Miguelito (Figure 1e), near San Luis Potosí (Labarthe-Hernández and Jiménez-López, 1992, 1994; Xu *et al.*, 2004, 2005). It is also well exposed in the Salinas (Figure 1d) and Zacatecas (Figure 1c) horsts (*e.g.*, Ponce and Clark, 1988;

Legend:

- Town ■
- Vein Y
- Normal fault (dashed where inferred)
- Trend of Cenozoic faults (dashed where inferred)

- Alluvium
- Intraplate mafic volcanic rocks: 1. Miocene; 2. Plio-Quaternary
- Tertiary felsic volcanic rocks
- Eocene red beds
- Tertiary granitic rocks
- Pre-Tertiary rocks

Peñón Blanco granite

Santa María fault system

Zacatecas

Sierra de San Miguelito

San Luis Potosí Graben

Villa de Reyes Graben

Enramadas Graben

Silva-Romo, 1993; Loza-Aguirre, 2005) and may extend to the Fresnillo, Sombrerete, and Durango regions (*e.g.*, Albinson, 1988; Gemmell *et al*., 1988; Nieto-Samaniego *et al*., 2005. See Figure 1b).

The regional NW-trending Río Santa María fault system divides the Mesa Central into two domains (Figures 1a, 1b) with contrasting stratigraphy and different geomorphic aspect. North of the system, Mesozoic marine sedimentary rocks are intruded by a few isolated felsic stocks of mid-Tertiary age. The mid-Tertiary volcanic cover has been nearly completely eroded. South of the system, the area is covered by a thick sequence of mid-Tertiary felsic volcanic rocks of the SMO. Both domains in the Mesa Central are crossed by a complex array of normal fault systems with ~NS, NW and NE trends.

Age relations among the fault systems in the southeastern part of the Mesa Central are ambiguous, as there are no systematic crosscutting relations among them throughout the region (Aranda-Gómez *et al*., 1989). In the horsts that form Sierra de Zacatecas (Figure 1c) and Sierra de Salinas (Figure 1d), NS-trending faults appear to be the youngest fault system, as they displace NW-trending faults within the horst. But the NE-trending Villa de Reyes graben, near San Luis Potosí, clearly postdates the NW-trending fault of Sierra Miguelito (Figure 1e). Precious and base metal mineralization is commonly located at or near the intersection of these fault systems.

Earlier work in the Pinos area suggested that the lava dome complex was emplaced above a faulted and tilted red bed sequence that was derived from deformed Mesozoic marine sedimentary and early Tertiary volcanic rocks (Aguillón-Robles *et al*., 1994). Based upon the stratigraphic position between folded Mesozoic rocks and felsic SMO volcanic rocks, a middle- to late Eocene age was assumed for the red beds (Aguillón-Robles *et al*., 1994, 1996). Lithologic similarities with other Eocene red conglomerates and volcanic rocks in the region (*e.g.*, Zacatecas red conglomerate: Edwards, 1955; Aranda-Gómez and McDowell, 1998) appear to support this conjecture.

In this study, several feldspar K-Ar dates for samples from the Pinos volcanic complex were obtained. These results, together with the documented field relations and magnetic polarity data in the volcanic units indicate that several episodes of volcanism, faulting and sedimentation occurred in the region between ~27 and 32 Ma.

GEOLOGIC SETTING

Regional setting

The Mesa Central province of central Mexico is an elevated plateau located near the southern end of the Basin and Range province. The stratigraphic sequence includes rocks from the Mesozoic to the Cenozoic. The Mesozoic sequence is exposed in several isolated ranges. Extensive outcrops of Mesozoic rocks occur for instance in the Sierra de Salinas, a ~NS horst located ~20 km northwest of Pinos (Figures 1b, 1d). Silva-Romo (1993) recognized three distinct stratigraphic packages separated by unconformities in the Mesozoic sequence of the Sierra de Salinas. The oldest package (late Triassic – middle Jurassic: Centeno-García and Silva-Romo, 1997) is formed by a thick succession of late Triassic turbidites (La Ballena Fm.) and a sequence of middle Jurassic andesites and polymictic conglomerates (Nazas Fm.). The middle package (late Jurassic) consists of limestone and siltstone (Zuloaga Fm.), phosphatic rock and chert (La Caja Fm.). The youngest set of units (Cretaceous) is formed by limestone (Taraises Fm.), limestone and chert (Tamaulipas Fm.), limestone, chert, and shale (Cuesta del Cura Fm.), argillaceous limestone and shale (Indidura Fm.), and volcaniclastic turbidites and shale (Caracol Fm.). The Mesozoic sequence Sierra de Salinas is intruded by several stocks of granitic composition (Figure 1d). These subvolcanic granites are highly distinctive as they contain muscovite and black tourmaline in veinlets, radial aggregates or irregular patches replacing the matrix or feldspar phenocrysts.

The Eocene red beds continental strata occur in several localities of the Mesa Central overlying folded Mesozoic rocks (*i.e.*, Guanajuato and Zacatecas mining districts, Figures 1a, 1b; Edwards, 1955; Aranda-Gómez and McDowell, 1998). They typically consist of coarse conglomerates. The tectonic setting where these rocks accumulated is still debated. They have been interpreted as molasse deposits accumulated in topographic lows after the Laramide Orogeny or as fanglomerates associated to post-Laramide normal faulting.

The most characteristic lithologies in the southern part of the Mesa Central are felsic volcanic rocks, which are part of the extensive Sierra Madre Occidental volcanic province, and locally overlie and/or intrude folded Mesozoic marine

Figure 1. Regional geologic setting and location of the Río Santa María fault system. a: The Pinos (P) volcanic complex is located near the southeastern end of the Sierra Madre Occidental volcanic province, in a region where it is unusually broad. Both in the Guanajuato (G) and Zacatecas (Z) mining districts there are thick sequences of Eocene red beds exposed between the folded Mesozoic rocks and the Tertiary volcanic rocks. Other localities cited in the text are A: Aguascalientes city; D: Durango city; F: Fresnillo; R: Santa María del Río; RC: Real de Catorce; S: Sombrerete; Sa: Salinas; SLP: San Luis Potosí city. The Mesa Central boundary is also shown. b: Generalized geologic map of the Mesa Central (simplified after Nieto-Samaniego *et al*., 2005) and location of the Santa María fault system. Note that west of Zacatecas the Mesa Central boundary coincides with the limit of the region almost completely covered by mid-Tertiary volcanic rocks. c: Distribution of NW-trending normal faults and veins within the NS-trending Sierra de Zacatecas horst (simplified after Loza-Aguirre, 2005). d: NW-trending normal faults and location of outcrops of Peñón Blanco granite within Sierra de Salinas horst (simplified after Silva-Romo, 1993). e: Domino-style fault system exposed in Sierra San Miguelito and location of the Enramadas, San Luis Potosí and Villa de Reyes grabens (simplified after Labarthe-Hernández *et al*., 1982).

rocks and a thick sequence of well-lithified continental red beds. The volcanic sequence exposed in the region between Zacatecas and San Luis Potosí is dominantly rhyolitic–rhyodacitic and includes numerous lava flows associated with extensive dome complexes and major ignimbrites. Isotopic age determinations throughout the Zacatecas–San Luis Potosí region yielded ages between 31 and 26 Ma (Labarthe-Hernández *et al.*, 1982; Nieto-Samaniego *et al.*, 1996). Older andesites (K-Ar: ~44 Ma; Labarthe-Hernández *et al.*, 1982) and felsic ignimbrites (K-Ar: 46.8 – 42.3 Ma; Ponce and Clark, 1988; Loza-Aguirre, 2005) occur locally at the base of the volcanic sequence. The younger orogenic volcanic rocks in the Zacatecas and San Luis Potosí region are broadly similar in age and composition to those in the Upper Volcanic Supergroup of the Sierra Madre Occidental near Durango City and the older andesites and ignimbrites to the Lower Volcanic Complex studied by McDowell and Keizer (1977) along a transect from Durango to Mazatlán.

Geology of the Pinos region

The Pinos region is located in the central part of Mexico, in the region between San Luis Potosí and Zacatecas (Figure 1a). Epithermal Au-Ag vein mineralization is related to the mid-Tertiary sequence formed by domes, associated lava flows and/or coulees, and ash-flow tuffs (Figure 2a). Part of the Mesozoic sequence is exposed around the flanks of the Pinos volcanic complex (Figure 2a). The Mesozoic is folded and overlain in angular discordance by clastic red beds, which we informally name the Pinos red beds. These red beds are formed by well-lithified conglomeratic sandstone and matrix-supported, generally fine-grained to medium-grained, polymictic conglomerate (Figures 2 and 3). Clasts in the Pinos red beds were derived from the Mesozoic basement (limestone + sandstone + shale + propylitized andesitc lavas), subaerial felsic volcanic rocks of unknown provenance, and tourmaline-bearing muscovite granite. Clast composition, size, and their relative abundance vary from one site to other.

The Pinos red beds are locally interlayered with subaerial felsic volcanic rocks, including ash-fall tuffs, at least one densely welded ash-flow tuff, and water-laid or reworked pyroclastic material. Colors of the conglomerate and sandstone in the red bed sequence depend on the relative abundance of the clasts. The sequence tends to be dark red in those sites where propilitized andesitic fragments are abundant, gray where limestone and chert clasts dominate, and yellow where ash-fall tuffs and volcaniclastic sediments are concentrated. Dip angles in the red bed sequence range between 20 and 30° in most places, and near major faults beds may be tilted as much as 70º due to fault drag (Figure 2b). A conservative estimate of the minimum thickness of the red bed sequence in northern part of the Pinos volcanic complex is 900 m.
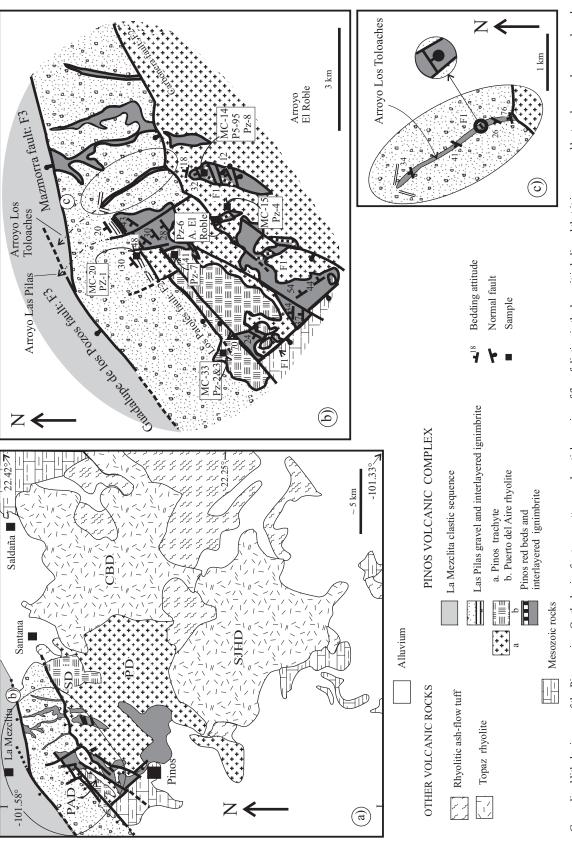
The lava flows associated with the Pinos volcanic complex occur above the Pinos red beds. In places the contact between the lava flows and the red beds is roughly concordant (Figure 3a) and both units are equally tilted to the north. In many sites the contact is a clear angular unconformity between the steeper Pinos red beds and the more gently dipping lavas (Figure 4).

In places the red bed sequence and/or the lavas of the dome complex are in fault contact (F2 in Figure 3a and Los Patoles and Carbonera faults in Figure 2b) with a coarse, clast-supported, generally unconsolidated gravel deposit we informally call Las Pilas gravel as it is well exposed along the Arroyo Las Pilas, north of Los Patoles fault system (Figure 2b). This gravel consists of clasts derived from the adjacent domes. Near the domes, Las Pilas gravel deposit dips up to 30º to the north or northwest. A few kilometers away from the domes, Las Pilas gravel deposit consists of alternating beds of gravel, gravely sand, and sand, and dips <10° to the northwest. Las Pilas gravel is also inter-layered with volcanic horizons, including ash-fall tuffs and a densely welded rhyolitic ash-flow tuff. The depositional contact between the Pinos red beds and Las Pilas gravel is marked by an angular unconformity. As in the case of the lava dome–red bed contact, the angle of unconformity is a function of the dip angle in the red bed strata. Tilting in the Pinos red beds resulted from displacement in a set of faults (F1 in Figures 2b and 3a), which are older than the dome complex and Las Pilas gravel deposit (Figures 2b, 2c, and 3a).

INTERPRETATION OF FIELD RELATIONS

Intrusive relations between the felsic lavas and the Pinos red beds were observed in few outcrops. Layering in the red conglomerate is disrupted and steeper near the igneous rock (Figure 5). These exposures are interpreted as feeder dikes for the dome complex. The dikes locally produced bleaching in the red beds. The structural disruption of the layering appears to have been caused by drag associated with magma injection and/or pre-intrusion normal faulting (Figure 3a).

On the basis of phenocryst mineralogy and whole rock chemical analyses (Aguillón-Robles *et al.*, 1996), two different lava types in the northwestern part of the volcanic complex were identified. A dark red, porphyritic, potassium-rich trachyte cropping near the town of Pinos is a unit we call the Pinos trachyte (Figures 2 a, 2b). This thick stack of lava flows contain 20–30% phenocrysts (sanidine, plagioclase and altered pyroxene) set in a felsic matrix (devitrified glass) stained with hematite, which gives the rock a distinctive dark red color. Sanidine phenocrysts are invariably resorbed (Figure 6a), and may be up to 6 mm long. Pyroxene is commonly altered, except in rare vitro-phyric samples. Plagioclase phenocrysts tend to be euhedral and sometimes form glomeroporphyritic aggregates with

Figure 2. a: Generalized lithologic map of the Pinos region. On the basis of outcrop patterns and partial mapping of flow foliation in the lavas it is believed that it is composed by two large endogenous lava domes: Pinos (PD) and Puerto del Aire (PAD). In addition to these volcanic structures, in the area occur other domes: Cerro Blanco (CBD), San Juan de los Herrera (SJHD), and Saldaña (SD). b: Geologic map of the northwestern portion of the Pinos volcanic complex. c: Geology along arroyo Los Toloaches. Note the presence of partially concealed normal faults in the red beds exposed in the arroyo bed, and the presence of an ignimbrite interlayered with Las Pilas gravel deposit. The maps show the locations of samples selected for radiometric (MC) dating as well as paleomagnetism (Pz).
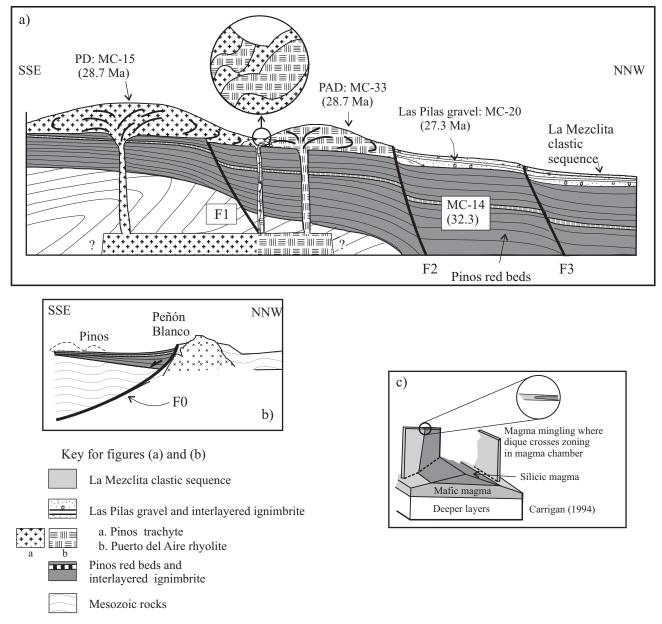
Figure 3. a: Idealized section that shows the stratigraphic and structural relations observed in the northwestern part of the Pinos and Puerto del Aire dome complexes. No scale. Inset: at the contact between the rhyolites and trachytes there is a zone where both lithologies are mingled. b: It is hypothesized that the red bed sequence observed in Pinos was accumulated on the hanging wall of an important listric normal fault during regional extension. The presence of clasts of tourmaline-bearing muscovite granite in the red beds suggests that the source area was near the Peñón Blanco stock, which is the only known outcrop of granite in the region. c: Simplified model for simultaneous emplacement of two felsic lava domes with different composition. Magma mingling occurs at the conduit as magma travels to the surface (afer Carrigan, 1994).

orthopyroxene. Sanidine is never included in these aggregates, and plagioclase and pyroxene crystals do not occur as inclusions in the K-feldspar.

The second lava type exposed in a dome (PAD: Figures 2 and 3) on the northwestern part of the complex is a buff-colored, porphyritic rhyolite. We call this unit the Puerto del Aire rhyolite, which has the mineral assemblage quartz > sanidine >> plagioclase + biotite > opaque minerals. Feldspar phenocrysts tend to be euhedral, and range in size from 1 to 3 mm. Beta quartz pseudomorphs are com-

monly embayed (Figure 6b). A micro- to cryptocrystalline felsic matrix (devitrified glass) forms ~80% of the rock. Biotite phenocrysts are seldom preserved; more often opaque minerals replace them.

Contact relations between the trachyte and rhyolite indicate that they were emplaced at least in part simultaneously. One body of banded lavas located at the contact of the trachyte and rhyolite domes contains thin (1–10 cm) contorted layers of red trachyte alternating with yellowish-white, high-silica rhyolite (Figure 7a).

Figure 4. Contact between the Pinos red beds and the Pinos trachyte. In this locality (UTM: 14Q0234424, 2470522) there is a clear angular unconformity.

Petrographic comparison between samples of both lithologies, collected at the gradational contact of trachyte and rhyolite domes, with rocks from the inner part of the volcanic structures indicates that there was significant mingling and mixing of the magmas at the thin-section scale (Figure 7b).

The occurrence of separate lava domes, formed either by trachyte or rhyolite, and banded lava at their contact layout raises the following questions: Where did the mingling occurred? and what is the age relation of the domes and the banded lava? Mingling at the surface of lavas simultaneously issued from two vents from independent magma chambers appears to be unlikely, as formation of the complex banding and folding shown in Figure 7 would be prevented by quenching and brecciation of the outer crust of the flows in the atmosphere. Thus, mingling probably occurred either in the magma chamber or in the volcanic conduit as the magma was ascending towards the surface (*e.g.*, Morrow and McPhie, 2000). In our view, the model proposed by Carrigan (1994) to explain compositional variations in the Inyo chain of domes at the Long Valley caldera may explain our observations in the Pinos volcanic complex. A single zoned magma chamber may have supplied all the magma types documented at the Pinos volcanic complex, providing that magma ascent occurred along a fracture and the roof of the chamber was slanted (Figures 3a, 3c). Simultaneous or sequential eruption (as the fracture propagated) along the length of a fracture with the right orientation may have produced the Pinos and Puerto del Aire domes, as well as the mixed lava in widened parts of the dike, which may have acted as cylindrical conduits near the surface. Our acceptance of Carrigan (1994) model implies that the lava domes
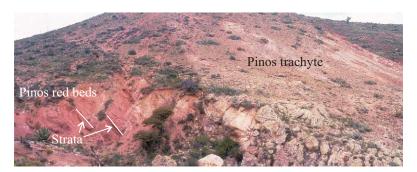

Figure 5. Intrusive contact relation between the Pinos red beds and the lavas of the Pinos trachyte (UTM: 14Q0235656, 2470959).

and banded lava formed simultaneously or during a short time span that can not be resolved with K-Ar technique.

There is evidence of several periods of normal faulting in the region. Arbitrarily, we consider as the most important deformation pulses those that in addition to the faults themselves have clastic deposits associated. We call these major pulses of deformation F1 to F3 (Figure 3). To other phase that is registered in the area only as faults with a small to moderate displacement we refer as F1' (the name of the immediately previous deformation pulse). Those faults inferred solely from coarse clastic deposits in the stratigraphic record, such as the Pinos red beds, without the existence of structures within the studied area, we refer as F0. The conspicuous ignimbrite in the red bed sequence is an excellent marker for locating the fault planes within this fanglomerate. In several localities, in the erosional windows formed by the arroyos (*e.g.*, Arroyo Los Toloaches in Figures 2b, 2c), is possible to follow NE-trending fault traces in the Pinos red beds, which outside of the window are buried by the

lava domes and Las Pilas gravel. These partially concealed faults (F1 in Figure 3a) are evidence of a deformation pulse prior to main period of volcanism in the area represented by the domes. The faulted contact between the lava domes and Las Pilas gravel (*i.e.*, along the ENE- to NE-trending Los Patoles and Carboneras fault systems in Figure 2b), which is made of clasts derived from the lava domes, is interpreted as a second period of faulting (F2, Figure 3a). This system locally displaces earlier NW-trending faults (F1') which affect the Pinos trachyte and the red bed sequence (Figure 2b). Here, NE F2 faulting is clearly younger than NW F1' faulting, but in other parts of Sierra Pinos NW-trending faults displace earlier ENE and NE-trending faults. As pointed out before, these kind of ambiguous age relations among Cenozoic fault systems are common throughout the southern portion of the Mesa Central.

Near the town of La Mezclita (Figure 2a), the tilted Las Pilas gravel deposit is in fault contact with horizontal sand and silt beds, we informally call La Mezclita clastic sequence. We consider the ENE-trending Mazmorra and Guadalupe de los Pozos faults (Figure 2b) as evidence of a third period of faulting (F3, Figure 3a). Close to this fault, in the footwall of the Mazmorra fault, the conglomeratic horizons of Las Pilas gravel deposit are firmly cemented with silica.

Regional tilting towards the northwest of the whole Paleogene continental sequence, with higher dip angles in the older rocks (Pinos red beds 54–12°, Figure 2b), compared with the younger Las Pilas gravel (30–10°, Figure 2b) and La Mezclita clastic sequence (~horizontal) can be interpreted as fanning caused by syn-depositional normal faulting.
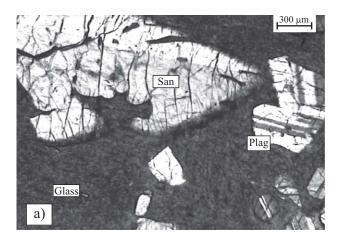
The general nature of the Pinos red bed sequence suggests that an important period of normal faulting may have occurred prior to F1. Detailed sedimentological analysis of the red beds in Guanajuato and Zacatecas led Edwards (1955) to conclude that these units, which occupy the same stratigraphic position as the Pinos red beds –between the folded Mesozoic and the mid-Tertiary volcanic sequences– were caused by "general uplift, block faulting, volcanism, and conglomerate deposition" after Laramide compression ceased in the region (Edwards, 1955, p. 182). However, as we have not been able to document normal faults older than F1 in the Pinos area, we refer to this hypothetical pulse of faulting as F0 (Figure 3b).

Overall tilt direction of the red bed sequence and Las Pilas gravel deposit suggests that the master fault associated with F0 should be north of Pinos. The presence of clasts of tourmaline-bearing muscovite granite in the Pinos red beds is consistent with this interpretation. The Peñón Blanco stock is the only known outcrop of muscovite and tourmaline granite in the area and it is located ~20 km to the N40W of the dome complex (Figures 1b, 1d). Therefore, the source area of the clasts in the fanglomerate, and the footwall of the master fault could be located in that direction. Fanning dips in the whole Tertiary continental sequence suggest

Figure 6. a: Sanidine phenocrysts in the Pinos trachyte are always deeply embayed, suggesting that they may be accidental. Cross polars. San: sanidine; Plag: plagioclase. b: Quartz (Qtz) phenocrysts in the Puerto del Aire rhyolite are resorbed, sanidine phenocrysts are smaller, and plagioclase crystals are rare. The matrix is microcrystalline and interpreted as devitrified glass.
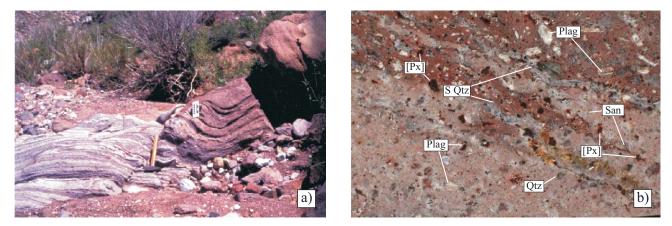
Figure 7. a: A key for the understanding of the age relation between the trachyte and rhyolite is the occurrence of banded lavas, where red layers of trachyte alternate with white rhyolite. The contorted nature of the banding and mingling observed in some layers indicates that both domes were emplaced at the same time and magma mingling occurred at the magma chamber or in the volcanic conduit. b: A closer view of the banded lava. Argillized plagioclase and altered pyroxene [Px] are conspicuous in the darker bands. Note the presence of isolated crystals of the same phases in the rhyolite. These crystals are interpreted as evidence of mixing of both magma types. Veinlets of secondary quartz (S Qtz) are roughly parallel to the banding in the rock. Polished rock slab 7×4.7 cm.

faulting contemporaneous with deposition and formation of a half(?)-graben as a depocenter.

We believe the observed and inferred pulses of deformation (F0 – F3) were related to the regional NW-trending Río Santa María fault system. It is evident that this system may have continuously acted while the Pinos continental sequence was accumulated, as indicated by NW-trending faults cut by and cutting NE and ENE-trending faults. Thus, the apparent pulsating nature of deformation (F0 – F3) at the Pinos region may be an artifact of an incomplete stratigraphic record.

TIMING OF THE GEOLOGIC EVENTS

These basic field relationships can be assembled into an ordered sequence of events in the form of a schematic time line to provide an interpretation of the geologic history of the northwestern portion of the Pinos volcanic complex and surrounding area (Figure 8). As a first approximation, the local events are loosely assigned to epochs in the geologic time scale, based on what is known about major tectonic events in central Mexico (de Cserna, 1989): 1) the end of compressional deformation associated with the Laramide orogeny (pre–late Eocene); 2) block faulting and accumulation of continental red bed sequences in central Mexico (Eocene – early Oligocene); and 3) development of the bulk of Upper Volcanic Sequence at the eastern portion of the Sierra Madre Occidental (middle Oligocene).

Sample selection

It is possible to further refine the timing of volcanism and faulting events using isotopic dating methods. Four

samples were chosen for dating using the K-Ar method (see Figure 2b for sample location). An additional sample collected at the Peñón Blanco stock was dated by the $^{40}Ar/^{39}Ar$ method. These samples were selected as representative of important events in the geologic history of the area (Figure 8) and the specimens were collected from outcrops where contact relations were unambiguous. In addition, they contain appropriate mineral phases for dating that are as close to their pristine form as possible. Effects of alteration, weathering, contact metamorphism and hydrothermal activity appear to be absent at outcrop and thin-section scale.

MC-35 is a sample of the Peñón Blanco granite (Figure 1d). This rock provides a crude estimate of the minimum age of Laramide deformation, as the shallow intrusive was emplaced in deformed marine sedimentary rocks. Its porphyritic texture, with beta quartz pseudomorphs and euhedral sanidine phenocrysts suggests that it is a high level, subvolcanic intrusion. Absence of penetrative fabrics associated with folding and/or shearing shows that it is post-tectonic with respect to compressional tectonics. The granite also provides a broad maximum age for deposition of the red bed sequence and the age of the hypothetical F0 period of faulting (Figure 8). Presence of granite clasts in the Pinos red beds indicates that they were incorporated in the alluvial fans that originated the red beds when the intrusive body was exhumed. Subaerial volcanic clasts in the red beds may have been derived from extrusive equivalents of this stock.

Sample MC-14 provides an age for the first known volcanic episode (V1, Figure 8) and, as an interbedded ignimbrite unit, a time point for the accumulation of the Pinos red beds. The same sample, together with MC-33, MC-15, and MC-20 establish age brackets for faulting pulses F1, F1', and F2. MC-20 provides the maximum age for F3 and a time point in the sedimentation of the post-dome gravels
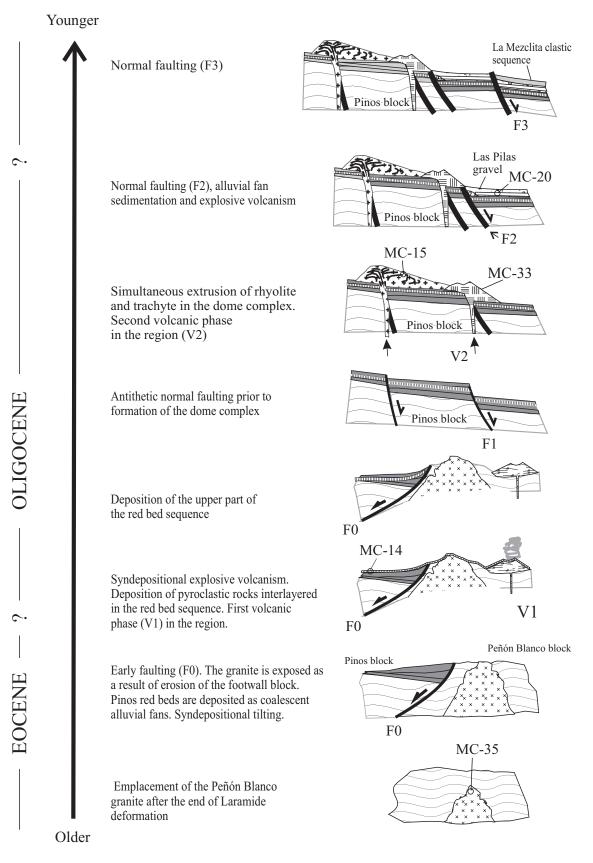
Aranda-Gómez et al.

Younger

Normal faulting (F3)

La Mezclita clastic sequence

Pinos block

F3

Normal faulting (F2), alluvial fan sedimentation and explosive volcanism

Las Pilas gravel

MC-20

Pinos block

F2

Simultaneous extrusion of rhyolite and trachyte in the dome complex. Second volcanic phase in the region (V2)

MC-15

MC-33

Pinos block

V2

Antithetic normal faulting prior to formation of the dome complex

Pinos block

F1

Deposition of the upper part of the red bed sequence

F0

Syndepositional explosive volcanism. Deposition of pyroclastic rocks interlayered in the red bed sequence. First volcanic phase (V1) in the region.

MC-14

F0

V1

Early faulting (F0). The granite is exposed as a result of erosion of the footwall block. Pinos red beds are deposited as coalescent alluvial fans. Syndepositional tilting.

Peñón Blanco block

Pinos block

F0

Emplacement of the Peñón Blanco granite after the end of Laramide deformation

MC-35

OLIGOCENE

EOCENE

?

?

Older

Figure 8. Schematic time line for the evolution of the Pinos volcanic complex. See text for discussion.

(Figure 8). Finally, samples MC-15 and MC-33 provide ages for the Pinos and Puerto del Aire domes.

Results

Age of the Peñón Blanco stock

Some of the most distinctive components of the Pinos red beds are well rounded clasts, up to 30 cm in diameter, of muscovite- and tourmaline-bearing granite. The only report-ed outcrop of granite in the vicinity is the Cerro del Peñón Blanco stock, 20 km to the northwest of the Pinos volcanic complex (Figures 1b, 1d). On the basis of the systematic change of the average diameter of the granite clasts, from 10 cm in the northern part of the Pinos volcanic complex to less than 5 cm in the southern part, we assume that the granite clasts in the red beds came from the stock. Therefore, the age of the granite sets an older limit to the time of deposition of the strata in the red conglomerate where they occur. Sample MC-35 is a granite porphyry collected at the stock (Figure 1d) with ~45% of phenocrysts set in very fine grained, felsic matrix that has hypidiomorphic-granular texture. Phenocryst assemblage is quartz $\geq$ sanidine > sodic plagioclase >> muscovite. Quartz crystals, both phenocrysts and in the matrix, have bipyramidal habit and some of the phenocrysts are embayed. Euhedral to subhedral feldspar crystals form glomeroporphyric aggregates up to 6 mm in diameter. Muscovite occurs both as phenocrysts (3–4 mm long) and in fine grained, randomly oriented masses. The fine-grained muscovite is interpreted as an alteration product that replaced irregular parts of the matrix and some of the feldspar phenocrysts. Tourmaline forms radial aggregates both in the matrix and within sanidine phenocrysts.

Previously, Mugica and Albarrán (1983) obtained a K-Ar age of 47 ± 4 Ma on muscovite from the granite (Figure 9). A $^{40}Ar/^{39}Ar$ step-heating experiment performed on muscovite phenocrysts yielded a plateau age of 50.94 ± 0.47 Ma (97.9% of ^{39}Ar) (Figures 9 and 10).

Age of the Pinos red beds

The ignimbrite interlayered with the Pinos red beds in the northern part of the complex (Figures 2b and 3a: MC-14) is a densely welded rhyolitic ash-flow tuff, ~8 m thick, with ~30% of phenocrysts up to 3 mm long. Matrix is slightly devitrified and preserves a good vitrophyric tex-ture. Glass shards and pumice are flattened, defining a clear eutaxitic fabric. Mineral paragenesis is: sanidine > quartz > plagioclase >> opaque minerals. Sanidine is unaltered and plagioclase is partially replaced by sericite. Some samples collected in this unit contain rare crystals of a mafic mineral (pyroxene?) completely replaced by bastite and opaques.

A whole-rock K-Ar date of 30.5 ± 1.5 Ma was previ-ously obtained in a commercial laboratory. We confirmed this result with a K-Ar date of 32.3 ± 1.5 Ma in a sanidine separate from sample MC-14, which was collected at the same site (Table 1). Uncertainties in both analyses are large
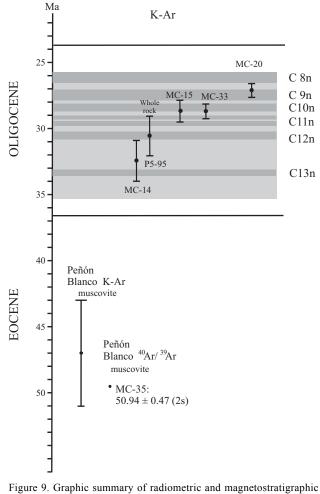

Figure 9. Graphic summary of radiometric and magnetostratigraphic results. Error bars equal one sigma analytical uncertainty in the age de-termination. The light/dark gray pattern corresponds to Cande and Kent (1995) magnetic polarity time scale for part of the Oligocene (series of chron C13 to C18). Normal polarity intervals are dark gray and labeled. The K-Ar age for the Peñón Blanco granite was obtained by Mugica and Albarrán (1983).

and the whole rock age clearly overlaps with other dates obtained from samples MC-15 and MC-33 collected in the volcanic domes of Pinos (Figures 2, 3, and 9).

Ages of the Pinos and Puerto del Aire domes and F1

The Pinos trachyte, represented by MC-15 (Figures 2 and 3), contain ~25% of phenocrysts in a felsitic, microc-rystalline groundmass. Phenocryst assemblage is sanidine > plagioclase >> hypersthene(?) >> opaque minerals >> apatite + zircon. Orthopyroxene is replaced by bastite and opaque minerals. Quartz is restricted to the matrix, where it forms very fine-grained granophyric intergrowths with K-feldspar. Opaque minerals also occur as granules dis-seminated throughout the matrix. They are always oxidized to hematite(?). Sanidine is anhedral, with deeply embayed boundaries. Euhedral plagioclase occurs as isolated crys-tals (~3–4 mm) or in glomeroporphyric aggregates with
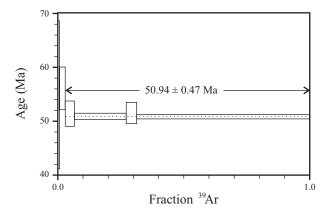
Figure 10. ^{40}Ar/^{39}Ar incremental heating spectra for muscovite in MC-35.

subordinated orthopyroxene. Both feldspars in the dated sample are unaltered, except for iron oxide staining along some cleavage planes.

MC-15 was collected at a site where the trachyte clearly buries a fault trace that cuts the Pinos red beds, truncating the interbedded ash-flow tuff. A K-Ar date for sanidine separated from the trachyte is 28.7 ± 0.9 Ma.

MC-33 (Figures 2 and 3) contains ~20% phenocrysts, up to 3 mm long, set in an aphanitic matrix that also contains randomly oriented sanidine microphenocrysts. A narrow and poorly developed rim of granophyre surrounds some partially resorbed beta quartz pseudomorphs. Well preserved, unaltered sanidine phenocrysts are euhedral to subhedral and commonly display Carlsbad twinning. The sample contains a small proportion of opaque minerals in opacite clusters that are interpreted as pseudomorphs after biotite. It is likely that the matrix is devitrified glass, as suggested by relatively coarsely crystalline spherulites seen in the section. Sanidine separated from sample MC-33 gave a K-Ar date of 28.7 ± 0.7 Ma. (Table 1, Figure 9).

Ages of the post-volcanic Las Pilas gravel deposit and F2

Sample MC-20 was collected from an ash-flow tuff interlayered with the tilted Las Pilas gravel deposit exposed to the north of the dome complex (Figures 2 and 3). It provides a minimum age for F2, is synchronous with the accumulation of part of the clastic deposit, and gives a maximum age for the youngest fault event (F3) recognized in the complex. The rock is a densely welded rhyolitic ash-flow tuff, ~6 m thick, with conspicuous lithophysae filled with quartz and chalcedony. Phenocrysts form ~35% of the rock and their paragenesis is quartz ≥ sanidine > plagioclase >> hypersthene(?) ≥ opaque minerals. The groundmass has a remarkably well-preserved eutaxitic fabric. Aside from the litophysae fillings there is no visible alteration in the phenocrysts. The rock also contains small lithic fragments with textures and mineralogy similar to the trachyte of the

Pinos dome (*cf.* MC-15). The dated sample (MC-20) was cleaned of lithic fragments by hand picking the crushed fragments under a binocular microscope prior to mineral separation. A K-Ar age for sanidine yielded 27.3 ± 0.6 Ma (Table 1, Figure 9)

PALEOMAGNETISM

Seven sites were selected for a paleomagnetic study (see Figure 2b for sample location) of representative igneous rocks of the Pinos volcanic complex; most of them are the same sites as sampled for geochronology. Six to ten oriented samples were gathered at each site using a gas-powered drill and oriented *in situ* with magnetic and solar compasses. Two sites were collected from the ignimbrite intercalated with the Pinos red beds (Pz-6/MC-14 and Pz-8); two sites were collected from rhyolites of the Puerto del Aire dome (Pz-2/MC-33 and Pz3), and one site was obtained from an

Table 1. Age determinations.

^{40}Ar/^{39}Ar data §

Sample	Material	Age method	Age (Ma)	±1s
MC-35	Mus	plateau	50.94	0.47

K-Ar data

Sample	Material	%K	^{40}Ar*	%Ar*	Age (Ma)	±1s
Ash flow tuff interlayered in the Pinos red beds						
MC-14	San	6.205	7.677	81	32.3	1.5
		6.191	7.710	72		
			8.404	78		
			7.620	87		
P5-95	wr	5.070	0.583	94.8	30.5	1.5
		4.920	0.585	95.1		
Pinos trachyte						
MC-15	San	8.660	9.450	91	28.7	0.9
		8.446	9.783	88		
			9.270	81		
			9.904	88		
Puerto del Aire rhyolite						
MC-33	San	4.864	6.414	76	28.7	0.7
		4.682	6.225	64		
			5.456	78		
Ash flow tuff interlayered in Las Pilas gravel						
MC-20	San	6.185	6.567	77	27.3	0.6
		6.265	6.660	72		
			6.677	66		
			6.691	68		

^{40}Ar/^{39}Ar analyses were done at Queen's University; decay constants: λ_β=4.963×10^{-10}/yr; λ_ε+$\lambda_{\varepsilon'}$=0.581×10^{-10}/yr; ^{40}K/K=1.167×10^{-4}; § Dates and J values for the intralaboratory standard (*e.g.*, MAC-83 biotite at 24.36 Ma) were referenced to TCR sanidine at 28.0 Ma. K-Ar analyses by Fred McDowell and Teledyne Isotopes (P5-95); ^{40}Ar* (×10^{-6} scc/g); %Ar*: percent radiogenic argon. Mus: muscovite; San: sanidine; wr: whole rock.

ignimbrite interlayered in Las Pilas gravel deposit (Pz-1/MC-20). In addition, one site was obtained from a trachyte assigned to the Pinos Dome at Arroyo El Roble (Pz-7). Finally, one site was collected from a trachyte flow of the Pinos Dome where it clearly overlies the Pinos red beds at the headwater of arroyo El Roble (Pz-4).

Samples were subjected to progressive alternating field (AF) or thermal demagnetization. Remanence measurements were done on a superconducting magnetometer (2G Enterprises) at the University of New Mexico or with a Digico spinner magnetomer at the Centro de Geociencias, Universidad Nacional Autónoma de México (UNAM). Interpretations of the vectorial composition of the remanence are based on visual inspection of orthogonal demagnetization diagrams (Zijderveld, 1967), principal component analysis was used to determine remanence directions, and standard spherical statistics were used to calculate site mean directions.

The remanent magnetization of all samples is relatively straightforward. Except for sites Pz-6 and Pz-8, the natural remanent magnetization (NRM) is univectorial (Figure 11), and is well defined by linear segments that trend to the origin but do not reach it. The NRM is of high coercivity, with median destructive fields in excess of 110 mT. Sites Pz-6 and Pz-8 contain a soft magnetization of random orientation possibly induced by lightning. Maximum unblocking temperatures exceed 525°C (the maximum temperature at which samples were treated).

The magnetization is interpreted as a TRM (thermoremanent magnetization) acquired upon cooling. The remanence carriers are both magnetite and hematite as suggested by IRM acquisition curves. Inspection under the petrographic microscope indicates that hematite and magnetite are primary magmatic phases, with some hematite formed by high temperature oxidation.

Mean paleomagnetic directions and associated statistical parameters are summarized in Table 2. In all cases, it is important to note that the characteristic magnetization is north directed and moderately steep positive (Figure 11). This suggests, but does not prove, that the units sampled
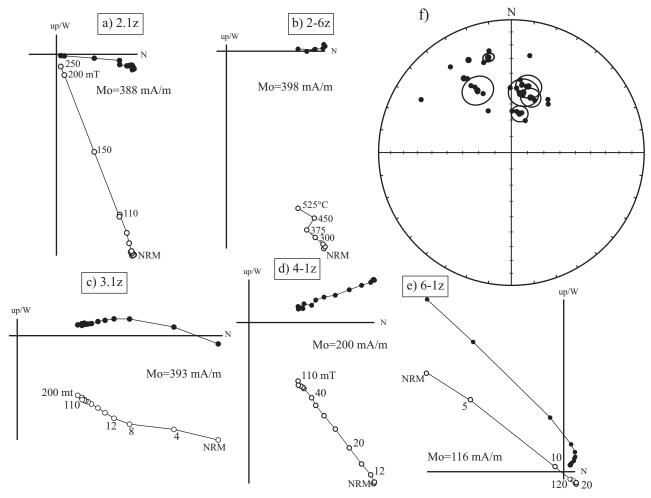

Figure 11. a-e: Orthogonal demagnetization diagrams for typical samples. The first digit in the sample label identifies the sites; for identification of rock units see Table 2. The examples are for samples subjected to AF demagnetization, except for (11b). Closed (open) symbols are projections in the horizontal (vertical) plane. Examples (c) and (e) show large overprints of low coercivity. f: Equal area stereographic projection of (*in situ*) site means with confidence intervals (large circles) and individual sample directions (small circles).

Table 2. Paleomagnetic data and statistical parameters for rocks of the Pinos volcanic complex.

Site	N	Rock Unit	dec	inc	k	α95	dec-tc	inc-tc
Pz-1	5	Ign. Las Pilas gr.	346.6	27.2	650.2	3.0	352.6	14.6
Pz-2	4	Puerto del Aire rhy.	12.1	65.6	336.2	5.0		
Pz-3	5	Puerto del Aire rhy.	14.8	47.4	105.7	7.5		
Pz-4	5	Pinos trachyte	11.6	51.9	75	8.9		
Pz-6	5	Ing. Pinos red bds.	331.6	45.8	70.1	9.2		
Pz-7	3	Pinos trachyte	19.5	53.9	427.9	6.0		
Pz-8	2	Ing. Pinos red bds.	328.1	34.2			336.7	25.8
Pz-11	2	Ing. Pinos red bds.	335.3	24.4			344.7	21.7

N is the number of samples demagnetized, dec (dec-tc) and inc (inc-tc) are the declination and inclination in *in situ* and tilt corrected coordinates, respectively. Alpha 95 and k are the precision parameter and the confidence region around the mean direction. Declinations and inclinations in tilt corrected coordinates are only available for outcrops that allow for direct measurement of bedding attitude. High inclinations of sites 2 through 7 suggest that these sites require a structural correction. Site Pz-11 is located in the southern part of the Pinos volcanic complex. Therefore, the location of this sample is not shown in Figure 2.

acquired their magnetization during a single interval of normal polarity.

DISCUSSION

This study comprises a collection of limited data sets, each of which alone cannot provide an unambiguous timing of the geologic history for the northern part of the Pinos volcanic complex. Together, however, they support a relatively complete depiction of the sequence and nature of geologic events.

Mapping has firmly established that the area contains three generations of continental clastic deposits, two of which (Pinos red beds and Las Pilas gravel deposit) probably accumulated in fault-bounded basins. Moreover, the eruption of trachyte and rhyolite domes and flows of the Pinos volcanic complex occurred during the same interval that clastic deposition was occurring and regional felsic ignimbritic volcanism produced planar deposits that are interlayered with the clastic sedimentary strata. Finally the field relations demonstrate that trachyte and rhyolite simultaneously erupted during the evolution of the Pinos and Puerto del Aire domes. However, the mapping does not resolve whether these domes were formed in a single eruption, and what physical and temporal relationship it has to the contiguous domes of Cerro Blanco and San Juan de los Herrera (Figure 2a). This precludes conclusions about the nature and tectonic controls of the source of these magmas.

The K-Ar data set is the most limited. Unusually large experimental uncertainties plague two of the four analyzed feldspars, but even with the typical one-sigma uncertain-

ties of <1 Ma, the results show only that volcanic activity preserved in the clastic sections and that of the Pinos domes was of mid-Tertiary (Oligocene) age. The four ages span about 5.5 m.y., but a liberal consideration of the uncertainties permits timing between 34 and 26.5 Ma. The K-Ar ages do not contradict the relative timing from field relationships, but that concordance is not surprising in view of the large analytical errors. Those errors do not allow resolution of the timing for the sequence of events evident in the field. At a minimum, the data clearly separate the ages of the muscovite-bearing Peñón Blanco granite and the volcanic section. The pluton certainly belongs to an earlier pulse of magmatism.

Notwithstanding these limitations in the data, several definitive implications may be drawn from their combined application. The 50.9 Ma age for the Peñón Blanco stock shows that Laramide shortening had ended in the region prior to that time. This age also gives a maximum time for the F0 faulting and for the erosion and deposition of the red bed strata where the granite clasts are included. Pinos red bed deposition continued until at least 28.7 Ma, the age for samples MC-15 and MC-33 (Table 1), collected at the lava domes. The combined range of the four K-Ar ages for the volcanic rocks (Table 1) fits well with the known timing of volcanism within the mid-Tertiary southeastern portion of the SMO, of which the Pinos volcanic complex is a part.

K-Ar ages for two phases of the Pinos dome lavas are both 28.7 Ma (Table 1). These results agree with the observation that trachyte and rhyolite erupted together. This assumes, of course, that a single time of eruption applies to the entire northern and western portion of the dome complex. An inference that is consistent with the intimate mingling of both lavas, which probably occurred in the volcanic conduit. MC-14 (32.2 Ma, Table 1) is, as expected on the basis of the stratigraphic relations, older than the dome complex and MC-20 (27.3 Ma, Table 1) is younger than the lava domes.

The magnetic polarity data for the volcanic rocks may possibly help to further constrain the probable age of the events. The time span of dated volcanism, 27.3 Ma to 32.3 Ma, includes five major reversals of magnetic polarity (*i.e.*, crons C13n to C9n; Cande and Kent, 1995). All of the samples measured for this study have normal magnetic polarity. Both K-Ar dating (calibration of reference samples) and magnetostratigraphic dating (curve fitting to independently dated time points, see Cande and Kent, 1992) are subject to calibration. Hence, comparisons between them are vulnerable to additional systematic errors. Nonetheless, all of the four K-Ar dated samples overlap with a normal polarity intervals within the analytical uncertainties of the ages (Figure 9). The age and uncertainty (27.3 ± 0.6 Ma) of the ignimbrite interlayered in the Las Pilas gravel deposit (MC-20) spans most of the normal polarity chron C 9n; therefore, we assume that the age of the rock must be between 27.0 Ma (the minimum age of chron C 9n: Cande and Kent, 1995) and 27.9 Ma (the maximum age of MC-20

considering the one sigma analytical uncertainty: Table 1). The age of the Pinos and Puerto del Aire domes must be between 27.8 and 29.6 Ma, a time span that includes the analytical uncertainties associated to both MC-15 and MC-33 (Table 1). However, only the normal chrons C 10n and C 11n.1n satisfy all the conditions for the time of emplacement of the domes (simultaneous, normal polarity, and within the time span 27.8 – 29.6 Ma). Therefore, we conclude that the most probable age for the formation of the dome complex is 28.3 – 29.6 Ma (C 10n – C 11n.1n, Cande and Kent, 1995). Finally, the age of the ignimbrite interlayered with the Pinos red beds may correspond to C 12n or C 13n, if the analytical uncertainties of both MC-14 and P5-95 are considered (Figure 9). Although both samples were collected at the same outcrop, were dated with the same method and have similar analytical uncertainties, the age of MC-14 was obtained from a sanidine concentrate, which is likely to yield a more reliable result. Therefore, we believe MC-14 is a better estimate of the real age of the rock and that C 13n further restrict the time span for its formation. Therefore, we believe that the age of the ignimbrite must lie between 33.1 (Cande and Kent, 1995) and 33.8 Ma (Table 1).

The Pinos data show that extension in some areas of the Mesa Central is older than previously considered (29–27 Ma: Nieto-Samaniego *et al.*, 1999) by at least 4 m.y. but probably more if F0 is considered. Extension is also slightly older than in the Guanajuato mining district (32–28 Ma: Henry and Aranda-Gómez, 1992). At least in the case of Pinos, volcanism was synchronous with extension, rather than slightly younger than it (Nieto-Samaniego *et al.*, 1999). The age of the ignimbrite interlayered with the Pinos red beds only gives a time marker in the red bed sequence, deposit of which is presumably associated to the F0 faulting, but it does not constrain the beginning of this early pulse of deformation. On the basis of the location of the Pinos volcanic complex with respect to the Río Santa María fault system (Figure 1b), the regional scale of the same, and evidence of unroofing of the Peñón Blanco stock, we believe that F0 was related and parallel to the Río Santa María fault system. Although we made no direct observations on the timing of the Río Santa María fault system, it appears that activity in the ENE- and NE-trending faults of events F1 to F3 alternated with faulting in the Río Santa María system. Thus, faulting along the Río Santa María fault system continued thrughout the time span between about 27 and 32 Ma. For the NS-trending system of the Mesa Central, the best estimate of the timing of activity is provided by the Taxco-San Miguel Allende fault system near the Mesa Central southern limit, where the San Miguel Allende fault is ~12 Ma (Pérez-Venzor, *et al.*, 1996).

ACKNOWLEDGMENTS

APPENDIX A. EXPERIMENTAL PROCEDURES FOR RADIOMETRIC DATING

Mineral separation was done at the laboratory at Centro de Geociencias (UNAM) using standard procedures that involve magnetic and heavy-liquid separation. Final selection of mineral grains was made by handpicking under a binocular microscope from fractions that ranged in size from 40–60 to 60–80 mesh. Sanidine separates of the volcanic rocks were analyzed using conventional K-Ar. A muscovite concentrate from the Peñón Blanco granite was dated with the $^{40}Ar/^{39}Ar$ method. $^{40}Ar/^{39}Ar$ analysis was done at the Geochronology Research Laboratory of Queen's University, Kingston, Ontario, Canada, and conventional K-Ar analyses were done at the University of Texas at Austin.

K-Ar

Potassium was determined by flame photometry, using lithium as an internal standard and sodium as a buffer. Standard deviations (1σ) derived from pooled replicate analyses are ±1% or less for alkali feldspars. Radiogenic argon was analyzed by isotope dilution utilizing on-line extraction and purification with a 3" gas-source mass spectrometer operated under computer control. Feldspar samples were heated by radiofrequency induction, ideally to above 1,600 °C. Feldspars were also mixed with an equal weight of young basalt to facilitate release of radiogenic argon from the resultant melt (McDowell, 1983). Typical reproducibility of radiogenic argon measurements for feldspars is ±2.0% at one standard deviation, based on pooled replicate measurements over an extended period of time. In some cases, disagreement among results of replicate analyses is far greater than predicted from these pooled data. Samples MC-14 and MC-33 are examples of this problem. More conservative precision estimates given for these samples are derived from their argon measurements only. In Table 1 all errors are based on combined Ar and K uncertainties and are given at one standard deviation.

^{40}Ar/ ^{39}Ar

Minerals together with flux monitors (standards, MAC-83 biotite), were wrapped in aluminum foil and the resulting disks were stacked into a 11.5 cm long and 2.0 cm diameter container, and then irradiated with fast neutrons in position 5C of the McMaster nuclear reactor (Hamilton, Ontario) for 14 hr. Groups of flux monitors (typically 12 in total) were located at *ca.* l cm intervals along the irradiation container, and J values for individual samples were determined by second-order polynomial interpolation. The J values are typically between *ca.* 0.003 and 0.03 and vary by <10% over the length of the capsule. No attempt was made to monitor horizontal flux gradients as these are considered to be minor in the core of the reactor.

The samples were mounted in an aluminum sample holder, beneath the sapphire view port of a small, bakeable, stainless steel chamber connected to an ultra-high vacuum purification system. Following an overnight bakeout at 200 °C, an 8W Lexel 3500 continuous argon-ion laser was used for total fusion of monitors and step-heating experiments. For total-fusion dating, the beam was sharply focused; for step heating, the laser beam was defocused to cover the entire sample. Heating periods were *ca.* 3 minutes at increasing power settings (0.25 to 7 W). The evolved gas, after purification using an SAES C50 getter (*ca.* 5 minutes), was admitted on-line to a MAP 216 mass spectrometer, with a Bäur Signer source and an electron multiplier (set to a gain of 100 over the Faraday cup). Blanks, measured routinely, were subtracted from the subsequent sample gas-fractions. The extraction blanks were typically <10×10^{-13}, <0.5×10^{-13}, <0.5×10^{-13}, and <0.5×10^{-13} cm^3 STP for masses 40, 39, 38, 37, and 36, respectively. At least 24 flux monitors (MAC-83 biotite, few grains each: Sandeman *et al.*, 1999) were individually degassed at 1,200°C.

Measured argon isotope peak heights were extrapolated to zero time and normalized to the ^{40}Ar/^{36}Ar atmospheric ratio (295.5) using measured values of atmospheric argon. They were also corrected for neutron-induced ^{40}Ar from potassium, ^{39}Ar and ^{36}Ar from calcium (using the production ratios of Onstott and Peacock, 1987), and ^{36}Ar from chlorine (Roddick, 1983). Dates and errors were calculated using formulas given by Dalrymple *et al.* (1981) and the constants recommended by Steiger and Jäger (1977).

Isotope correlation analysis was based on the formulas and error propagation of Hall (1981) and the regression of York (1969). Errors shown in Table 1 and on the age spectrum represent the analytical precision at 2σ, assuming that the errors in the ages of the flux monitors are zero. This is suitable for comparing within-spectrum variation and for determining which steps constitute a plateau (McDougall and Harrison, 1988, p. 89). A conservative estimate of the error in the J value is 0.5%, and this should be added for inter-sample comparison. The dates (integrated/plateau) and J values for the intralaboratory standard (*e.g.*, MAC-83 biotite at 24.36 Ma) were referenced to TCR sanidine at 28.0 Ma (Baksi *et al.*, 1996).

We define a plateau age as the weighted mean of the apparent ages of at least three consecutive steps, comprising a minimum of 70% of the ^{39}Ar$_k$ released, which agree within 2 σ with the integrated age of the plateau segment. We further define a pseudoplateau as an age meeting similar statistical criteria to a plateau age, but that is composed of steps comprising 50–70% of the total ^{39}Ar$_K$ released.

REFERENCES

Aguillón-Robles, A., Aranda-Gómez, J.J., Marín-Solís, J.D., 1994, Noticia acerca de la presencia de sedimentos continentales y volcanismo asociado (¿Eoceno?) en la región de Pinos, Zac.: GEOS, 14(5), 80.

Aguillón-Robles, A., Rodríguez-Ríos, R., Leroy, J.L., Aranda-Gómez, J. J., 1996, Geología y características geoquímicas del centro volcánico de Pinos, Zac: Actas INAGEQ, 2, 3-8.

Aguirre-Díaz, G.J., McDowell, F.W., 1993, Nature and timing of faulting and synextensional magmatism in the southern Basin and Range, central-eastern Durango, Mexico: Geological Society of America Bulletin, 105, 1435-1444.

Albinson, T.F, 1988, Geologic reconstruction of paleosurfaces in the Sombrerete, Colorada and Fresnillo districts, Zacatecas State, Mexico: Economic Geology, 83, 1647-1667.

Aranda-Gómez, J.J., McDowell, F.W., 1998, Paleogene extension in the southern Basin and Range province of Mexico: Syndepositional tilting of Eocene red beds and Oligocene volcanic rocks in the Guanajuato Mining District: International Geology Review, 40(2), 116-134.

Aranda-Gómez, J.J., Aranda-Gómez, J.M., Nieto-Samaniego, A.F., 1989, Consideraciones acerca de la evolución tectónica durante el Cenozoico de la Sierra de Guanajuato y la parte meridional de la Mesa Central: Universidad Nacional Autónoma de México, Instituto de Geología, Revista, 8(1), 33-46.

Aranda-Gómez, J.J., Henry, C.D., Luhr, J.F, McDowell, F.W., 1997, Cenozoic volcanism and tectonics in NW Mexico a transect across the Sierra Madre Occidental volcanic field and observations on extension related magmatism in the southern Basin and Range and Gulf of California tectonic provinces, *in* Aguirre-Díaz, G.J., Aranda-Gómez, J.J., Carrasco-Nuñez, G., Ferrari, L., (eds.) Magmatism and tectonics in the central and northwestern Mexico. A selection of the 1997 IAVCEI General Assembly excursions: México, Universidad Nacional Autónoma de México, Instituto de Geología, 41-84.

Aranda-Gómez, J.J., Henry, C.D., Luhr, J.F., 2000, Evolución tectonomagmática post-paleocénica de la Sierra Madre Occidental y de la porción meridional de la provincia tectónica de Cuencas y Sierras, México: Boletín de la Sociedad Geológica Mexicana, 58(1), 59-71.

Baksi, A.K., Archibald, D.A., Farrar, E., 1996, Intercalibration of ^{40}Ar/^{39}Ar dating standards: Chemical Geology, 129, 307-324.

Cande, S.C., Kent, D.V., 1992, A new geomagnetic polarity time scale for the late Cretaceous and Cenozoic: Journal of Geophysical Research, 97, 13917-13951.

Cande, S.C., Kent, D.V., 1995, Revised calibration of the geomagnetic polarity time scale: Journal of Geophysical Research, 100(B4), 6093-6095.

Carrigan, C.R., 1994, Two-component magma transport and the origin of composite intrusions and lava flows, *in* Ryan M.P. (ed.), Magmatic systems: San Diego, California, Academic Press: 319-354.

Centeno-García, E., Silva-Romo, G., 1997, Petrogenesis and tectonic evolution of central Mexico during Triassic-Jurassic time: Revista Mexicana de Ciencias Geológicas, 14(2), 244-260

Dalrymple, G.B., Alexander, Jr. E.C., Lanphere, M.A, Kraker, G.P., 1981, Irradiation of samples for $^{40}Ar/^{39}Ar$ dating using the Geological Survey TRIGA Reactor: United States Geological Survey, Professional Paper, 1176, 1- 55.

de Cserna, Z., 1989, An outline of the geology of Mexico, *in* Bally, A.W., Palmer, A.R. (eds.), The Geology of North America –An overview, Volume A: Boulder, The Geological Society of America, 233-264.

Edwards, J.D., 1955, Studies of some early Tertiary red conglomerates of central Mexico: United States Geological Survey, Professional Paper, 264-H, 153-183.

Ferrari, L., López-Martínez, M., Rosas-Elguera, J., 2002, Ignimbrite flare-up and deformation in the southern Sierra Madre Occidental, western Mexico: Implications for the late subduction history of the Farallon plate: Tectonics 21(4), 17-1 – 17-24.

Gemmell, B.J., Simmons, S.F., Zantop, H., 1988, The Santo Niño silver-lead-zinc vein, Fresnillo District, Zacatecas, Mexico: Part I. Structure, vein stratigraphy, and mineralogy: Economic Geology, 83, 1597-1618.

Hall, C.M., 1981, The application of K-Ar and $^{40}Ar/^{39}Ar$ methods to the dating of recent volcanics and the Laschamp event: University of Toronto, Ph.D. thesis, 186 p.

Henry, C.D., Aranda-Gómez, J.J., 1992, The real southern Basin and Range: mid- to late Cenozoic extension in Mexico: Geology, 20, 701-704.

Labarthe-Hernández, G., Jiménez-López, L.S., 1992, Características físicas y estructura de lavas e ignimbritas riolíticas en la Sierra de San Miguelito, S.L.P: Universidad Autónoma de San Luis Potosí, Instituto de Geología, Folleto Técnico, 114, 1-34.

Labarthe-Hernández, G., Jiménez-López, L.S., 1994, Geología de la porción sureste de la Sierra de San Miguelito: Universidad Autónoma de San Luis Potosí, Instituto de Geología, Folleto Técnico, 120, 1-31.

Labarthe-Hernández, G., Tristán, M., Aranda-Gómez, J. J., 1982, Revisión estratigráfica del Cenozoico de la parte central del Estado de San Luis Potosí: Universidad Autónoma de San Luis Potosí, Instituto de Geología y Metalurgia, Folleto Técnico, 85, 1-208.

Labarthe-Hernández, G., Tristán-González, M., Aguillón-Robles, A., 1987, Cartografía geológica 1:50,000 Hoja Salitrera, S.L.P: Universidad Autónoma de San Luis Potosí, Instituto de Geología y Metalurgia, Folleto Técnico, 94, 1-85.

Labarthe-Hernández, G., Tristán-González, M., Aguillón-Robles, A., Jiménez-López, L.S., 1989, Cartografía geológica 1:50,000 de las hojas El Refugio y Mineral El Realito, Estados de San Luis Potosí y Guanajuato: Universidad Autónoma de San Luis Potosí, Instituto de Geología, Folleto Técnico, 112, 1-85.

Loza-Aguirre, I., 2005, Estudio estructural de la actividad cenozoica del sistema de fallas San Luis Potosí-Tepehuanes de la región Zacatecas-San José de Gracia: México, Instituto Tecnológico de Ciudad Madero, BSc thesis, 95p.

McDougall, L., Harrison, T.M., 1988, Geochronology and thermochronology by the $^{40}Ar/^{39}Ar$ method: New York, Oxford University Press, 1-269.

McDowell, F.W., 1983, K-Ar dating: Incomplete extraction of radiogenic argon from alkali feldspar: Isotope Geoscience (Chemical Geology), 1, 119-126.

McDowell, F.W., Keizer, R.P., 1977, Timing of mid-Tertiary volcanism in the Sierra Madre Occidental between Durango City and Mazatlan, Mexico: Geological Society of America Bulletin, 88, 1479-1486.

Morrow, N., McPhie, J., 2000, Mingled silicic lavas in the Mesoproterozoic Gawler Range volcanics, South Australia: Journal of Volcanology and Geothermal Research, 96, 1-13.

Mugica, R., Albarrán, J., 1983, Estudio petrogenético de las rocas ígneas y metamórficas del Altiplano Mexicano: Instituto Mexicano del Petróleo, Reporte interno C-1156.

Nieto-Samaniego, A.F, Alaniz-Alvarez, S.A, Camprubí í Cano, A., 2005, La Mesa Central: estratigrafía, estructura y evolución tectónica cenozoica: Boletín Sociedad Geológica Mexicana, 57(3), 285-318.

Nieto-Samaniego, A.F., Macías-Romo, C., Alaniz-Alvarez, S.A., 1996, Nuevas edades isotópicas de la cubierta volcánica cenozoica de la parte meridional de la Mesa Central, Mexico: Revista Mexicana de Ciencias Geológicas, 13(1), 117-122.

Nieto-Samaniego, A.F., Ferrari, L., Alaniz-Alvarez, S.A., Labarthe-Hernández, G., Rosas-Elguera, J., 1999, Variation of Cenozoic extension and volcanism across the southern Sierra Madre Occidental volcanic province, Mexico: Geological Society of America Bulletin, 111, 347-363.

Onstott, T.C., Peacock, M.W., 1987, Argon retentivity of hornblendes: A field experiment in a slowly cooled metamorphic terrane: Geochimica et Cosmochimica Acta, 51, 2891-2904.

Orozco-Esquivel, M.T., Nieto-Samaniego, A.F., Alaniz-Alvarez, S.A., 2002, Origin of rhyolitic lavas in the Mesa Central, Mexico, by crustal melting related to extension: Journal of Volcanology and Geothermal Research, 118(1-2), 37-56.

Pérez-Venzor, J.A., Aranda-Gómez, J.J., McDowell, F.W., Solorio-Munguía, J.G., 1996, Geología del Volcán Palo Huérfano, México: Revista Mexicana de Ciencias Geológicas, 13(2), 174-183.

Ponce, B.F., Clark, K. F., 1988, The Zacatecas mining district: A Tertiary caldera complex associated with precious and base metal mineralization: Economic Geology, 83, 1668-1682.

Roddick, J. C., 1983, High precision intercalibration of $^{40}Ar/^{39}Ar$ standards: Geochimica et Cosmochimica Acta, 47, 887-898.

Sandeman, H.A., Archibald, D.A., Grant, J.W., Villeneuve, M.E., Ford, F.D., 1999, Characterization of the chemical composition and $^{40}Ar/^{39}Ar$ systematics of intralaboratory standard MAC-83 biotite, *in* Radiogenic Age and Isotopic Studies: Geological Survey of Canada, Report 12, Current Research 1999-F, 13-26.

Silva-Romo, G., 1993, Estudio de la estratigrafía y estructuras tectónicas de la Sierra de Salinas, Estado de San Luis Potosí y Zacatecas: México, Universidad Nacional Autónoma de México, MSc thesis, 144 p.

Steiger, R.H., Jager, E., 1977, Subcommission on geochronology: Convention on the use of decay constants in geo- and cosmochronology: Earth and Planetary Science Letters, 36, 359-362.

Xu, S-S., Nieto-Samaniego, A.F., Alaniz-Álvarez, S.A., 2004, Tilting mechanisms in domino faults of the Sierra de San Miguelito, central Mexico: Geologica Acta 2(1), 189-201.

Xu, S-S., Nieto-Samaniego, A.F., Alaniz-Álvarez, S.A., 2005, Power-law distribution of normal fault displacement and length and estimation of extensional strain due to normal faults: A case study of the Sierra de San Miguelito, Mexico: Acta Geologica Sinica, 79(1), 36-49.

York, D., 1969, Least squares fitting of a straight line with correlated errors: Earth and Planetary Science Letters, 5, 320-324.

Zijderveld, J.D.A., 1967, A.C. demagnetization of rocks: Analysis of results, *in* Collison, D.W., Creer, K.M., Runcorn, S.K. (eds.), Methods in Rock Magnetism and Paleomagnetism: Amsterdam, Elsevier, 254-286.